

Phase Crossover induced by Dynamical Many Body Localization in Periodically Driven Long-Range Spin Systems

Mahbub Rahaman,¹ Takashi Mori,² and Analabha Roy¹

¹Department of Physics, The University of Burdwan, Golapbag, Bardhaman - 713 104, India

²RIKEN CEMS, 2-1 Hirosawa, Wako, Saitama, 351-0198, Japan

Dynamical many-body freezing occurs in periodic transverse field-driven integrable quantum spin systems. Under resonance conditions, quantum dynamics causes practically infinite hysteresis in the drive response, maintaining its starting value. We extended this to non-integrable many body systems by reducing the Hamiltonian symmetries through a power-law dependence in spin exchange energy, $J_{ij} = 1/|i - j|^\beta$. The dynamics of the integrable short-range Transverse Field Ising Model (TFIM) and non-integrable long-range Lipkin Meshkov-Glick (LMG) models were investigated. In the LMG, the resonance conditions in the driving field suppresses the heating postulated by the *Eigenstate Thermalization Hypothesis* (ETH) by inducing *Dynamical Many Body Localization*, or DMBL. This is in contrast to Many Body Localization (MBL), which requires disorder to suppress ETH. DMBL has been validated by the Inverse Participation Ratio (IPR) of the quasi-stationary Floquet modes. While TFIM has IPR localization for all drive parameters, the LMG exhibits high-frequency localization only at the resonances. IPR localization in the LMG deteriorates with an inverse system size law at lower frequencies, which indicates heating to infinite temperature. Furthermore, adiabatically increasing frequency and amplitude from low values raises the Floquet state IPR in the LMG from nearly zero to unity, indicating a phase crossover. This occurrence enables a future technique to construct an MBL engine in clean systems that can be cycled by adjusting drive parameters only.

Keywords: Dynamical localization, Thermalization, Phase Crossover

Periodically driven Quantum Many Body Systems can experience Dynamical Freezing (DMF) when dynamical hysteresis stops observables from reaching their diagonal averaged values and thermalizing to infinite temperature [1–3]. Under certain resonance conditions in the drive parameters, DMF can cause the response to ‘freeze’ completely to its initial value at all times. This arises as a consequence of additional approximate symmetries that occur at resonance. DMF has been demonstrated via the Rotating Wave Approximation (RWA) in the driven TFIM with nearest-neighbour interactions [4] and is shown to be protected when translational invariance is explicitly broken (say, by disorder) [5, 6].

The utilization of Floquet theory simplifies the analysis of time-periodic systems. For closed quantum systems governed by the time-dependent Schrödinger equation, the *Floquet Hamiltonian* allows for a mapping of the time-dependent dynamics into the dynamics of a time-independent effective Hamiltonian, provided the system is strobed at integer multiples of the time period of the drive. The time independent eigenstates of the effective Hamiltonian correspond to quasi-stationary *Floquet Modes* of the original Hamiltonian. The temporal progression of the system comes from phase coefficients that capture the dynamics [7, 8].

Any sufficiently complex non-integrable Many Body System is expected to thermalize according to the Eigenstate Thermalization Hypothesis (ETH) despite

the fact that closed quantum dynamics preserves the memory of the initial state of the system. This arises due to the properties of the matrix elements of observables in typical states[9]. The ETH can be readily adapted to time-periodic systems using Floquet theory (the Floquet-ETH, or FETH). Nonetheless, the conditions for ETH to hold are not particularly strong, and the density matrix of the system can fail to approach one that is described by a thermal expression. In such cases, the system is said to undergo *Many Body Localization* (MBL)[10]. This phenomenon is stable against local perturbations, and constitutes an exotic state of matter with far-reaching implications in theoretical physics, as well as in practical applications[11].

The addition of disorder has been identified as a crucial component in the onset of MBL. In that case, thermalization is prevented by disorder-induced localization. Nonetheless, alternative approaches to MBL in strongly interacting disorder-free systems [12–14], inhomogeneous systems [15–18], and by inducing disorder in the emergent physics [19] and by other effective means [17] (albeit with strong finite-size effects), have been reported. An alternative approach to realizing MBL in disorder-free *homogeneous* many-body systems involve *Floquet Engineering*, where a time-periodic drive is introduced, and the drive parameters tuned to introduce a clustering of quasistationary energies in a manner similar to localization[9].

In this article, we propose that additional approximate symmetries can be Floquet-engineered in quan-

67 tum many body systems with lower symmetry than
 68 the TFIM, such as those with long-range interactions.
 69 This results in both DMF and MBL occurring simul-
 70 taneously at resonant values of the drive parameters,
 71 and complete thermal behaviour at other values. This
 72 phenomenon is distinct from DMF in the TFIM, since
 73 clean TFIM systems, being integrable, never thermal-
 74 ize.

75 To demonstrate the onset of MBL, we investigate
 76 the driven Lipkin-Meshkov-Glick (LMG) model[20-
 77 25], a long-range system that is a special case of the
 78 more general Curie-Weiss model, wherein the nearest-
 79 neighbour exchange in the TFIM is extended to longer
 80 ranges with a power law dependence, $J_{ij} \sim 1/|i-j|^\beta$
 81 [26-28]. Setting $\beta = \infty$ recovers the TFIM, and set-
 82 ting $\beta = 0$ yields the LMG model. We have recovered
 83 the onset of DMF in this system and have supported
 84 our result with numerical simulations.

85 In addition, we compare the degree of localization
 86 of the quasi-stationary Floquet modes in both limits of
 87 β . In order to do so, we look at the Inverse Partici-
 88 pation Ratio (IPR) of the Floquet modes in the repre-
 89 sentation given by the eigenstates of the symmetry-
 90 breaking field. The IPR, closely related to the concept
 91 of quantum purity, is defined as the formal sum of the
 92 square of the density in some physically meaningful
 93 space or representation. A high IPR of a stationary
 94 state denotes low participation in most of the repre-
 95 sentation, and a low IPR distributes participation uni-
 96 formly across the representation, leading to ergodic
 97 dynamics[29]. Thus, IPR [30] is a useful tool for wit-
 98 nessing MBL of a quantum system. For an MBL sys-
 99 tem, the IPR is unity, and it scales inversely with the
 100 system size when it is thermally distributed [31].

101 In the first section of this paper, we present all es-
 102 sential theoretical frameworks. Our results for the
 103 LMG model are presented next in section II. In that
 104 section, we have used the Rotating Wave Approx-
 105 imation (RWA) [32], where only the slowest rotating
 106 terms in the Fourier expansion of the Hamiltonian in
 107 a frame co-rotating with the symmetry breaking drive
 108 field are retained. In addition, we have obtained
 109 analytical expressions for the Floquet modes and their
 110 IPR. They are used to probe the system dynamics in
 111 the high and low-frequency domains at both limits of
 112 β . In section III we have used phase space plots to
 113 contrast the low and high frequency limits of the LMG
 114 model in the thermodynamic limit by mapping it to an
 115 equivalent classical Hamiltonian system. Finally, in
 116 section IV, we have looked at numerical computations
 117 of the IPR of the Floquet modes for different values of
 118 the drive parameters, well beyond those that allow for
 119 the RWA. We observed that, if the system is driven by
 120 an adiabatically increasing drive frequency from low
 121 to high limit while remaining in the resonance region,

122 a sharp crossover from a thermal to an MBL phase
 123 occurs. We conclude with discussions and outlook.

I. BACKGROUND

125 The Eigenstate Thermalization Hypothesis (ETH) is
 126 a series of conjectures that allows for the thermaliza-
 127 tion of an isolated quantum many body system. The
 128 state of the system, $|\psi(t)\rangle$, evolves according to the
 129 Schrödinger equation $\hat{H}|\psi(t)\rangle = i\frac{\partial}{\partial t}|\psi\rangle$. The Hamilto-
 130 nian \hat{H} is assumed to be *non-integrable*, in that it lacks
 131 an extensive number of *local* additive conserved quan-
 132 tities, that is to say, there are no set of observables
 133 \hat{O}_s such that $\hat{H} = \sum_s \hat{O}_s$ for any extensive index s .
 134 Here, the \hat{O}_s constitute an arbitrary CSCO (complete
 135 set of commuting observables) that are *local*, having
 136 sub-extensive support in the system size. In addition,
 137 we postulate the existence of an equivalent Hamilto-
 138 nian \hat{H}_{eq} for every Hamiltonian \hat{H} as well as an "equi-
 139 librium" value A_{eq} for every observable \hat{A} , such that

$$A_{eq}(E) \equiv \frac{\text{Tr}(\hat{A}e^{-\beta\hat{H}_{eq}})}{\text{Tr}(e^{-\beta\hat{H}_{eq}})}, \quad (1)$$

140 where $E = \langle\psi(t)|\hat{H}|\psi(t)\rangle$ is the conserved energy of
 141 the system, and $\beta = 1/(k_B T)$ is the inverse tempera-
 142 ture, H_{eq} is an effective Hamiltonian that captures the
 143 long-time average dynamics of the system, and k_B is
 144 the Boltzmann constant.

To put it simply, ETH proposes that this many-
 body Hamiltonian undergoes thermalization as seen
 in the *long-time averages* of observables, with the
 eigenstates bearing resemblance to thermal states.
 The aforementioned hypothesis serves as a valuable
 instrument for comprehending the conduct of stim-
 ulated quantum systems and their correlation with
 thermal equilibrium. This assertion can be justified
 by examining the expectation value of an observable
 \hat{A} as it evolves under the Schrödinger equation. To
 see this, we first expand the state of the system $|\psi(t)\rangle$
 as:

$$|\psi(t)\rangle = \sum_m c_m(t) |m(0)\rangle,$$

145 where $|m(0)\rangle$ represents the eigenstates of $\hat{H}(0)$ with
 146 energy E_m . The coefficients $c_m(t)$ describe the time-
 147 dependent amplitude of the expansion. Plugging
 148 these expansions into the expression for the expec-
 149 tation value, we obtain the long-time average of the
 150 expectation value [33]:

$$\overline{\langle \hat{A}(t) \rangle} = \sum_{m,k} \overline{c_m^*(t)c_k(t)} \langle m(0)|\hat{A}|k(0)\rangle, \quad (2)$$

151 where the overline indicates the following operation
 152 for any time-dependent quantity $\mathcal{O}(t)$,

$$\overline{\mathcal{O}} \equiv \lim_{t \rightarrow \infty} \frac{1}{t} \int_0^t d\tau \mathcal{O}(\tau). \quad (3)$$

Had the system been integrable, the large number of conserved quantities would restrict mixing between the states during unitary evolution. In the non-integrable case, the system explores the entire Hilbert space spanned by eigenstates with eigenvalues close to E more-or-less uniformly. In that case, the matrix elements $\langle m(0) | \hat{A} | k(0) \rangle$ are said to satisfy the Srednicki ansatz [34, 35]:

$$\langle m(0) | \hat{A} | k(0) \rangle \approx A_{eq} \left(\frac{E_m + E_k}{2} \right) \delta_{mk} + e^{-\frac{1}{2}S\left(\frac{E_m+E_k}{2}\right)} f \left(\frac{E_m + E_k}{2}, E_m - E_k \right) R_{mk}. \quad (4)$$

Here, S is the thermodynamic entropy and R_{mk} are elements of a random matrix with vanishing mean and unit variance. What this means for the ensuing dynamics is that the system explores the accessible Hilbert space uniformly, and the matrix elements $\langle m(0) | \hat{A}(t) | k(0) \rangle$ become indistinguishable for most pairs of m and k . Applying this ansatz and taking the thermodynamic limit by ignoring terms $\mathcal{O}(e^{-S/2})$, the expression for the expectation value becomes:

$$\begin{aligned} \overline{\langle \hat{A}(t) \rangle} &\approx \sum_m \overline{|c_m(t)|^2} A_{eq} \left(\frac{E_m + E_k}{2} \right) \\ &\approx A_{eq}(E) \sum_m \overline{|c_m(t)|^2} = A_{eq}(E), \end{aligned}$$

153 where, in the last step, we utilized the fact that A_{eq} is
 154 a smooth function, and that the states with energies
 155 far from E have $|c_m(t)|^2 \approx 0$. Therefore, in the limit of
 156 large systems the expectation value of an observable
 157 \hat{A} is approximately equal to the thermal expectation
 158 value A_{eq} . This is the essence of the ETH, which sug-
 159 gests that individual eigenstates of a quantum system
 160 can be described by statistical mechanics in the long-
 161 time limit.

162 We now generalize the ETH to non-integrable many
 163 body systems that are closed, but not isolated. In
 164 that case, it is possible to impart a periodic time-
 165 dependence on the Hamiltonian while still ensuring
 166 unitary evolution. If the time period of the drive
 167 is T , and the corresponding drive frequency $\omega \equiv$
 168 $2\pi/T$, the Floquet theorem states that the solutions to
 169 the Schrödinger equation can be written as $|\psi(t)\rangle =$
 170 $e^{-i\epsilon t/\hbar} |\phi(t)\rangle$, where the $|\phi(t)\rangle$ are T -periodic states
 171 called *Floquet Modes*, the corresponding $\epsilon \in \mathbb{R}$, are
 172 called *quasienergies*. Quasienergy values are not
 173 unique, and can be made to be bounded within a Flo-
 174 quet photon, viz. a range $[-\omega/2, \omega/2]$ [36, 37]. As a

175 consequence, the unitary evolution operator can be
 176 split into two parts as follows [38].

$$U(t) = e^{-i\hat{K}_F(t)} e^{-i\hat{H}_F t}. \quad (5)$$

177 Here, the micromotion operator $\hat{K}_F(t)$ is time-periodic
 178 in T , with $\hat{K}_F(0) = 0$, and the Floquet Hamiltonian
 179 $\hat{H}_F = \hat{H}(t) - i \frac{\partial}{\partial t} \Big|_{t=T}$. Thus, if the system is strobed at
 180 integer multiples of T only, then the unitary evolution
 181 matches that of a time independent Hamiltonian H_F .
 182 This can capture most of the exact dynamics at large
 183 frequencies.

184 In such systems, the Floquet Eigenstate Thermaliza-
 185 tion Hypothesis (FETH) posits that, subject to specific
 186 conditions and in the context of a system of signifi-
 187 cant size, the Floquet modes themselves exhibit ther-
 188 mal state-like behavior, i.e., $\hat{H}_{eq} \approx \hat{H}_F$ in eqn 1. How-
 189 ever, in contrast to the isolated systems, the loss of
 190 energy conservation allows for the mixing of all Flo-
 191 quet modes in the ensuing dynamics, not just those
 192 with quasienergies near E . Were this to actually hap-
 193 pen in the ensuing dynamics, it can be reconciled with
 194 ETH [39] by ensuring that $\beta = 0$ in eq 1. In other
 195 words, the nonequilibrium steady state of the system
 196 tends to an infinite temperature, maximum entropy
 197 density matrix.

198 However, drive parameters like amplitude, fre-
 199 quency, and duty-cycle strongly affect the structure
 200 of the Floquet modes $|\phi\rangle$. Thus, they can be engi-
 201 neered to prevent the kind of full mixing that would
 202 lead to infinite temperatures, manifesting suppres-
 203 sion of thermalization dynamically. Thus, this type
 204 of *Floquet Engineering* can produce *Dynamical Many*
 205 *Body Localization* (DMLB), where the system fails
 206 to reach thermal equilibrium and remains localized,
 207 possibly near its initial state, even at large times.
 208 This paradigm seems similar to standard Many-Body
 209 Localization[40, 41], where disorder, locality, and in-
 210 tegrability can cause athermalism via breakdown in the
 211 Srednicki ansatz. However, DMLB is a purely dynami-
 212 cal phenomenon, and thus can occur regardless of dis-
 213 order, locality of observables, or system integrability,
 214 all of which have been studied for MBL onset [42–44].

Integrable Many Body systems do not exhibit thermalization. When subjected to time-periodic drives, Floquet engineering allows for the introduction of additional approximate conserved quantities that dynamically suppress the evolution of certain observables by hysteresis. This type of *freezing* of response has been shown in integrable systems [6]. A paradigmatic example is the driven Transverse Field Ising model (TFIM) in one dimension [45]. The Hamiltonian

is given by

$$\hat{H}(t) = \hat{H}_0 + h_z(t) \hat{H}_1, \quad (6)$$

$$\hat{H}_0 = -\frac{1}{2} \sum_{i=1}^N \sigma_i^x \sigma_{i+1}^x, \quad (7)$$

$$\hat{H}_1 = -\frac{1}{2} \sum_{i=1}^N \sigma_i^z. \quad (8)$$

Here, the undriven Hamiltonian \hat{H}_0 consists of nearest-neighbour interactions between N number of spin-1/2 particles on a one-dimensional spin network. The transverse field is denoted by \hat{H}_1 , and is being varied by a time-periodic and harmonic signal $h_z(t) = h_0 + h \cos \omega t$, yielding a time period $T = 2\pi/\omega$ with amplitude h , drive frequency ω , and d.c. field h_0 . This Hamiltonian can be readily transformed into a spinless pseudo-fermionic system via the Jordan-Wigner transformation [4]. When written in momentum space spanned by spinors $\psi_k = (c_{-k}, c_k^\dagger)^T$ of fermions at momentum k created (annihilated) by operators c_k^\dagger (c_k), the effective Hamiltonian

$$H(t) = \sum_{(k,-k)-\text{pairs}} \psi_k^\dagger \left[\left(f_k - h_z(t) \right) \tau_z + \tau_x \Delta_k \right] \psi_k, \quad (9)$$

where $f_k = J \cos k$, $\Delta_k = J \sin k$, τ_{xyz} are the three Pauli Matrices, and the sum is over distinct $(k, -k)$ Cooper Pairs. We can transform our system to a frame that rotates with the time-varying symmetry-breaking field. This is achieved by the means of the unitary transformation operator

$$U(t) = \prod_k U_k(t) \quad (10)$$

$$U_k(t) = \exp \left\{ \left[\frac{ih}{\omega} \sin \omega t \right] \tau_z \right\}.$$

The resulting transformed Hamiltonian $H'(t) = U^\dagger(t) H(t) U(t) - iU^\dagger(t) \partial_t U(t)$ simplifies to

$$H'(t) = \sum_{(k,-k)-\text{pairs}} \psi_k^\dagger \left[\tau_z f_k + \tau_x \cos(\eta \sin \omega t) + \tau_y \sin(\eta \sin \omega t) \right] \psi_k, \quad (11)$$

where we defined $\eta = 2h/\omega$. Using the Jacobi-Anger formula [46]

$$e^{i\eta \sin \omega t} = \sum_{n=-\infty}^{\infty} J_n(\eta) e^{in\omega t}, \quad (12)$$

where $J_n(\eta)$ are Bessel Functions, the transformed Hamiltonian simplifies to

$$H'(t) = \sum_{(k,-k)-\text{pairs}} \psi_k^\dagger \left\{ \tau_z f_k + 2\tau_x \Delta_k \sum_{n \geq 0} J_{2n}(\eta) \cos(2n\omega t) - 2\tau_y \Delta_k \sum_{n \geq 0} J_{2n+1}(\eta) \sin[(2n+1)\omega t] \right\} \psi_k. \quad (13)$$

In the frequency regime $\omega \gg f_k$, the long-time average $H^{RWA} \equiv \lim_{n \rightarrow \infty} \frac{1}{nT} \int_0^{nT} dt H'(t)$ can serve as a suitable approximation for $H'(t)$. This approximation, known as the *Rotated Wave Approximation* (RWA), eliminates the oscillating modes and results in an effective Hamiltonian that is independent of time,

$$H^{RWA} = \sum_{(k,-k)-\text{pairs}} \psi_k^\dagger \left[f_k \tau_z + 2J_0(\eta) \Delta_k \tau_x \right] \psi_k. \quad (14)$$

It is evident that by manipulating the drive parameters, specifically the amplitude denoted by h and the frequency denoted by ω , in a manner such that η is positioned on a root of $J_0(\eta)$, the fermion number can be conserved to a significant extent at this particular resonance. Consequently, it is feasible to exercise direct control over H^{RWA} , resulting in a comprehensive suppression of the dynamics of otherwise responsive observables.

This phenomenon is highly general in nature, and can be readily adapted to non-integrable systems. In such cases, freezing has the additional effect of inducing DMBL, suppressing thermalization to infinite temperatures. Numerical quantification of localization of a specific (quasi) stationary state in a physically significant representation can be achieved through the computation of the *Inverse Participation Ratio* (IPR). In the position representation, the IPR for a state $|\psi\rangle$ [47–50] is defined as

$$\phi_{IPR} \equiv \int d\mathbf{x} |\langle \mathbf{x} | \psi \rangle|^4.$$

This definition can be generalized to the IPR of a state $|\phi\rangle$ in a representation given by complete orthonormal basis $|m\rangle$ as

$$\phi_{IPR} \equiv \sum_m |\langle m | \psi \rangle|^4. \quad (15)$$

The smallest value of the IPR corresponds to a fully de-localized state, $\psi(x) = 1/\sqrt{N}$ for a system of size N [50, 51]. Values of the IPR close to unity correspond to localized states [52]. For a periodically driven system, we look at the IPR of the quasi-stationary Floquet modes at $t = T$, where $t = 2\pi/\omega$ for drive frequency ω .

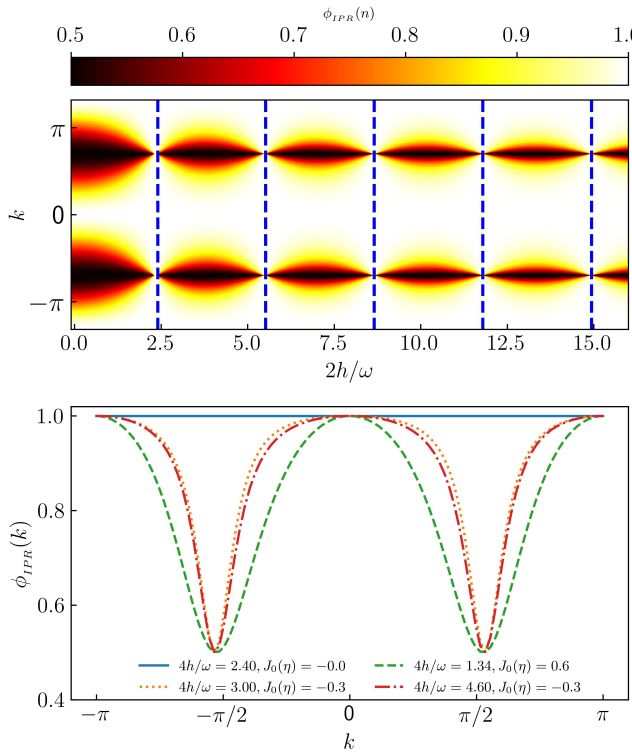


FIG. 1. Reduced IPR (defined in equation 16) for one of the two Floquet modes obtained from the exact dynamics of the TFIM for size $N = 100$ and $\omega = 90$ for the entire Brillouin zone (top panel, ordinate) and a few drive amplitudes (top panel, abscissa). The dashed lines (top panel) indicate the roots of $J_0(\eta)$. The bottom panel shows cross-sections for four different chosen amplitudes.

In the TFIM model, equation 14 indicates that, at resonance, when $J_0(\eta) = 0$, the Floquet modes are approximately given by the fermionic Fock states, which have a trivially unit IPR in the representation of the eigenmodes of the transverse field \hat{H}_1 in equation 6. Here, a particular Floquet mode can be decomposed into a direct product of cooper-pair states as $|\phi\rangle = \prod_{k,-k} |\phi_k^n\rangle$. In the RWA limit and at resonance, $|\phi_k^n\rangle$ has values of $|0\rangle, |k, -k\rangle$ for two values of $n = 0, 1$ respectively. We define the reduced IPR of $|\phi_k^n\rangle \forall k$ to be

$$\phi_{IPR}^{(n)}(k) = |\langle 0|\phi_k^n\rangle|^4 + |\langle +k, -k|\phi_k^n\rangle|^4, \quad (16)$$

where $n = 0, 1$. In the RWA limit and at resonance, this quantity is unity, indicating very low participation and the onset of freezing. Figure 1 shows results from numerically simulating the TFIM dynamics. The reduced IPR for a particular Floquet mode recovered by simulating the exact Schrödinger dynamics over a single time period of the drive, and plotted as a function of momentum k for different η 's. At resonance, when η lies at the root of the Bessel function $J_0(\eta)$,

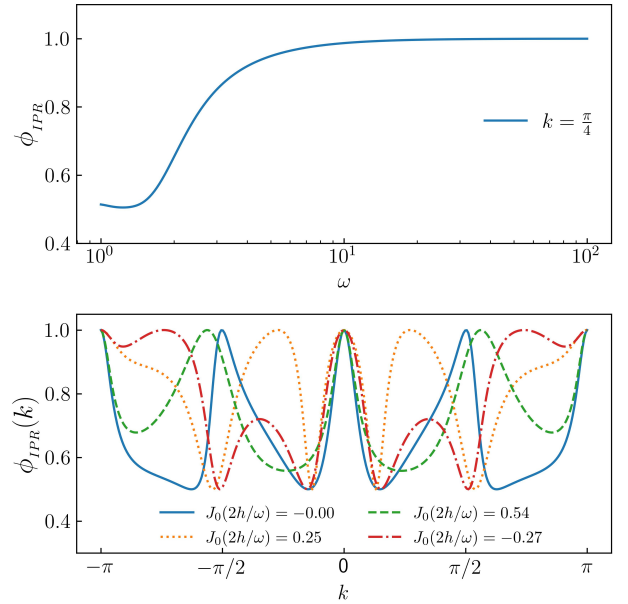


FIG. 2. Reduced IPR obtained by adiabatically increasing ω (top panel abscissa) for one the floquet mode obtained from equation 16 at the root of $J_0(\eta)$ for $N = 500$. IPR is ~ 0.5 (localized yet not fully freezing) upto $\omega \sim 2$, after that, smoothly increased to unity (fully localized and freezing) at higher $\omega \geq 10$ (top panel, ordinate). At bottom panel cross-sections for four chosen amplitudes at $\omega = 2$ are plotted for a brillouin zone (abscissa) with corresponding reduced IPRs (ordinate).

the IPR is exactly unity for all momenta. Outside this resonance, the IPR is unity only for some momenta because the effective Hamiltonian is perfect diagonal at $k \in \{-\pi, 0, \pi\}$ as can be seen in the cross-sectional plots of figure 1. As we move away from the resonance point, IPR reduces from unity. However, as the TFIM is an integrable spin model, the IPR never drops to a value that is small enough to indicate thermalization. At low frequencies, RWA fails due to the unavailability of zero off-diagonal terms in the effective transformed Hamiltonian, as well as the absence of integrability breaking terms to counteract the off diagonal terms. Consequently, the IPR remains quite high (~ 0.5) even at the resonance point as can be seen figure 1. At low frequency, this is valid for all momentum and parameter η , see figure 2.

Because the dependence of observable expectations on the eigenstates is always fairly strong for integrable systems like the TFIM, such systems will never exhibit any kind of thermal behaviour unless integrability breaking terms (such as strong disorder) are included [6]. As a result, it is not physically meaningful to refer to the unit IPR region as "Many Body Localization", because the parameter space lacks a thermal-

²⁹⁸ ized region to contrast with this state. The type of Flo-
²⁹⁹ quet Engineering described above, on the other hand,
³⁰⁰ can be easily applied to a broad class of nonintegrable
³⁰¹ systems where FETH is expected to hold in certain re-
³⁰² gions. Long-range spin systems, in particular, where
³⁰³ the exchange energies between far-off spins are taken
³⁰⁴ into account in the model Hamiltonian, are good can-
³⁰⁵ didates because they are known to thermalize when
³⁰⁶ driven with low frequencies [53].

³⁰⁷ II. LONG RANGE INTERACTIONS: THE LIPKIN ³⁰⁸ MESHKOV GLICK MODEL:

³⁰⁹ The periodically driven Curie-Weiss model for N
³¹⁰ long-range spins is described by the Hamiltonian

$$\hat{H}(t) = \hat{H}_0 + [h \cos(\omega t) + h_0] \hat{H}_1. \quad (17)$$

³¹¹ Here, the undriven part \hat{H}_0 and the driven part \hat{H}_1 are,
³¹² respectively,

$$\begin{aligned} \hat{H}_0 &= \frac{1}{2} \sum_{ij} J_{ij} \hat{\sigma}_i^z \hat{\sigma}_j^z, \\ \hat{H}_1 &= \sum_{i=1}^N \hat{\sigma}_i^x. \end{aligned} \quad (18)$$

³¹³ The Heisenberg exchange energy of the bond between
³¹⁴ spins i and j is given by

$$J_{ij} = \frac{J_\alpha}{N^{1-\alpha}} \frac{1}{r_{ij}^\alpha}, \quad (19)$$

with r_{ij} representing the smallest graph distance between them. Putting $\alpha = 0$ yields the Lipkin Meshkov Glick (LMG) model with all-to-all interactions $J_{ij} = J_0/N \forall (i, j), i \neq j$ [20, 54]. We choose to maintain the extensivity of the interaction energy by enforcing the condition

$$\frac{J_0}{N} \sum_{i \neq j} 1 = \frac{J_0}{N} \frac{N(N-1)}{2} = 1,$$

³¹⁵ yielding the Kac-norm $J_0 = 2/(N - 1)$. The
³¹⁶ Hamiltonian in equation 17 commutes with $P_{ij} \equiv$
³¹⁷ $\frac{1}{2} (1 + \vec{\sigma}_i \cdot \vec{\sigma}_j)$. In addition, it also commutes with
³¹⁸ the total angular momentum $S^2 = |\vec{S}|^2$, where $\vec{S} =$

³¹⁹ $S^x \hat{x} + S^y \hat{y} + S^z \hat{z} \equiv \frac{1}{2} \sum_i \vec{\sigma}_i$. We now choose to pop-
³²⁰ ulate the system in a state with $S^2 = \frac{N}{2} \left(\frac{N}{2} + 1 \right)$.
³²¹ In that case, the dynamics remains invariant in the
³²² $N + 1$ -dimensional space spanned by the common
³²³ eigenstates of $P_{ij}, |S|^2$ and S_z ; the so-called *Totally*
³²⁴ *Symmetric Subspace*, or TSS [55]. Let the eigenvalues
³²⁵ of S^z in the TSS be s_n , and the eigenvectors be $|s_n\rangle$.
³²⁶ Here, $s_n = -\frac{1}{2} + \frac{n}{N}$ and the index $n = 0(1)N$ has $N + 1$
³²⁷ values. The dynamics is restricted to this invariant
³²⁸ subspace, wherein the matrix elements of the Hamil-
³²⁹ tonian are given by

$$\begin{aligned} \langle s_i | \hat{H}_0 | s_j \rangle &= -\frac{4}{N-1} s_i^2 \delta_{ij}, \\ \langle s_i | \hat{H}_1 | s_j \rangle &= \left[\sqrt{\frac{N}{2} \left(\frac{N}{2} + 1 \right) - N s_i (N s_{i+1}) \delta_{i+1,j}} \right. \\ &\quad \left. + \sqrt{\frac{N}{2} \left(\frac{N}{2} + 1 \right) - N s_i (N s_{i-1}) \delta_{i-1,j}} \right]. \end{aligned} \quad (20)$$

³³⁰ These allow for a numerical representation of the
³³¹ Hamiltonian in the TSS.

³³² Next, we transform the Hamiltonian to the rotated
³³³ frame given by the operator

$$\hat{U}(t) = \exp \left[i \frac{h}{\omega} \sin(\omega t) \hat{H}_1 \right]. \quad (21)$$

³³⁴ This is analogous to the rotation performed for the
³³⁵ TFIM in eqns 10 and 11. Defining $\tau = \frac{h}{\omega} \sin \omega t$, we use
³³⁶ the fact that $\hat{H}_1 = 2S^x$, as well as the following iden-
³³⁷ tity obtained by using the Baker-Campbell-Hausdorff
³³⁸ formula,

$$e^{i2\tau \hat{S}^x} \hat{S}^z e^{-i2\tau \hat{S}^x} = \hat{S}^z \cos(2\tau) + \hat{S}^y \sin(2\tau), \quad (22)$$

to simplify the transformed Hamiltonian $\tilde{H}(t) = \hat{U}^\dagger(t) \hat{H}(t) \hat{U}(t) - \hat{U}^\dagger(t) \partial_t \hat{U}(t)$, yielding

$$\begin{aligned} \tilde{H}(t) &= -\frac{1}{N-1} \left[(S^z)^2 (1 + \cos 4\tau) + (S^y)^2 (1 - \cos 4\tau) \right. \\ &\quad \left. + \{S^y, S^z\} \sin 4\tau \right] - 2h_0 S^x. \end{aligned} \quad (23)$$

³³⁹ Next, we define $\eta \equiv 4h/\omega$ and use the Jacobi-Anger
³⁴⁰ formula in eqn 12 to expand $\tilde{H}(t)$. Ignoring constant
³⁴¹ terms, this yields

$$\tilde{H}(t) \sim \frac{(\hat{S}^x)^2}{N-1} - 2h_0\hat{S}^x - \frac{J_0(\eta)}{N-1} \left[(\hat{S}^z)^2 - (\hat{S}^y)^2 \right] - \frac{2}{N-1} \sum_{k=1}^{\infty} J_{2k}(\eta) \left[(\hat{S}^z)^2 - (\hat{S}^y)^2 \right] \cos(2k\omega t) - \frac{2}{N-1} \sum_{k=1}^{\infty} J_{2k-1}(\eta) \{ \hat{S}^y, \hat{S}^z \} \sin[(2k-1)\omega t]. \quad (24)$$

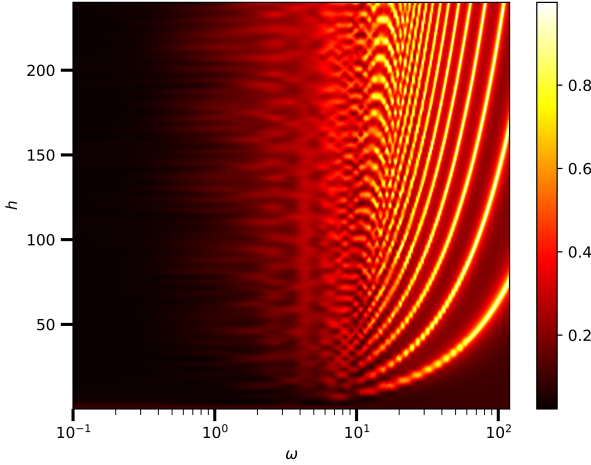


FIG. 3. Plot of the numerically averaged IPR (IPR computed using eqn 27) in the TSS plotted in the $h - \omega$ plane for $N = 100$ spins. In order to display the thermalized region more clearly, ω is plotted on a logarithmic scale on the abscissa. Note that, since the IPR is clearly non-negative, an average IPR of zero means that all Floquet states have zero IPR. Furthermore, the boundedness of IPR in $\phi_{IPR}(n) \leq 1$ ensures that if the average IPR is unity, then all Floquet states have unit IPR.

If ω is large enough to smooth out the harmonic components, we obtain the RWA,

$$\tilde{H}(t) \approx \tilde{H}_{\text{RWA}} \equiv \frac{(\hat{S}^x)^2}{N-1} - 2h_0\hat{S}^x - \frac{J_0(\eta)}{N-1} \left[(\hat{S}^z)^2 - (\hat{S}^y)^2 \right]. \quad (25)$$

If the drive amplitude h is adjusted such that η lies at a root of $J_0(\eta)$ (the localization point), the RWA Hamiltonian is diagonal in the representation of the transverse field \hat{S}^x , yielding an IPR of unity in that representation, similar to the TFIM in the previous section. Note however, that if the DC transverse field h_0 is set to 0, then, at the localization point, the RWA Hamiltonian $\tilde{H}_{\text{RWA}} \sim (\hat{S}^x)^2$. The eigenvalues are two-fold degenerate. This produces infinitely many (Floquet) eigenmodes in the degenerate subspace whose IPRs may not always be unity in the S^x representation. The removal of this degeneracy necessitates the inclusion

of the d.c. field h_0 . However, note that rational values of h_0 may add accidental degeneracies in \tilde{H}_{RWA} . To see this, note that, at a localization point, the eigenvalues of \tilde{H}_{RWA} in the TSS are given by

$$\text{Eigs}[\tilde{H}_{\text{RWA}}] = \frac{\left(\frac{N}{2} - m\right)^2}{N-1} - 2h_0\left(\frac{N}{2} - m\right), \quad (26)$$

where the half-integer $-N/2 \leq m \leq N/2$ is the eigenvalue corresponding to a particular eigenstate $|m\rangle$ of the symmetry-breaking field \hat{S}^x . In order to ensure that no additional degeneracies occur, we have to set h_0 in such a way that no two energies accidentally coincide. If $N \gg 1$ (substantially large), then this condition can be readily met by assuring that $(1 - 2h_0)^{-1}$ is never an integer that is divisible by N . To ensure this in our numerical simulations, we have kept h_0 at a small irrational value. The localization of the Floquet states at resonance is supported by exact numerical results, as can be seen in the phase diagram fig 3. Here, we have plotted the arithmetic mean over all Floquet states of the IPR in the TSS for each point in the $h - \omega$ plane for $N = 100$ spins. The IPR in S^x representation is

$$\phi_{IPR}(n) = \sum_m |\langle m | \phi^n \rangle|^4. \quad (27)$$

As can be readily seen in the figure, the IPR is essentially zero when $\omega \lesssim 1$. There is considerable structure in the phase diagram for larger drive frequencies, and along the lines given by the roots of $J_0(\eta)$, the IPR is essentially unity, in agreement with eqn. 25.

In figure 4, we show plots of the IPR of the Floquet modes $|\phi^n\rangle$ for $S^2 = (N/2)(N/2+1)$. These plots were obtained numerically by diagonalizing the propagator $U(t)$ at $t = T$, where $U(t)$ is defined in eqn 5. This propagator was obtained from simulations of the exact quantum dynamics using QuTiP, the Quantum Toolbox in Python [56]. We kept the frequency at a fairly large value $\omega = 90$ where we expect that RWA would be valid, and $N = \mathcal{O}(10^2)$. The density plot in the upper panel of fig 4 depicts the IPR of the Floquet states; the abscissa $\eta = 4h/\omega$ and the ordinate is $n/(2N+1)$, where $n \leq 2N$ is a non-negative integer that indexes the Floquet states in increasing order of m . The dashed vertical lines correspond to the roots

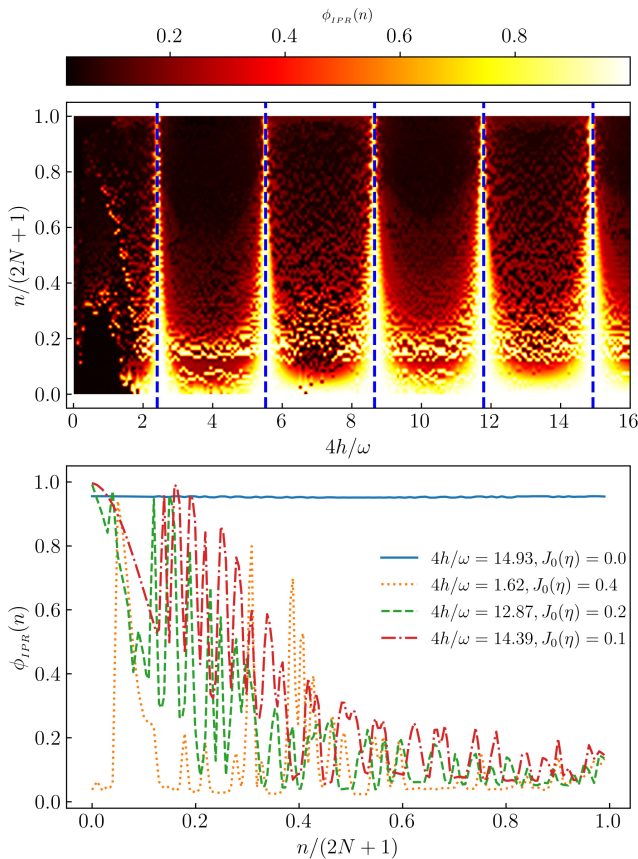


FIG. 4. IPR density plot for all possible Floquet modes (top panel ordinate) for different values of $\eta = 4h/\omega$ (top panel abscissa), deduced from equation 27 for exact LMG Hamiltonian for $N = 50$. Blue dashed lines are roots of $J_0(\eta)$. At bottom panel cross-section of IPR (ordinate)for four different η 's plotted for all possible floquet modes(bottom panel, abscissa) at $\omega = 90$. IPR founds to be \sim unity for all Floquet modes at roots of J_0 .

of $J_0(\eta)$. Comparing with the IPR of the TFIM in fig 1, we can see a very similar patterns in the immediate neighbourhood of the roots. Evidently, the IPR approaches a value of one for sufficiently large values of the roots, strongly suggesting full DMBL. Deviations occur at the smallest root of $J_0(\eta)$ (around $\eta = 2.405$) due to the contributions from higher order terms in eq 24. Thus, a higher root is favored for DMBL.

The bottom panel of fig 4 contains cross sections of the full IPR plot for selected values of η as indicated in the legend. When the drive amplitude h is adjusted such that η is close to a root of $J_0(\eta)$, the Floquet States are mixed, but not entirely thermal, since the IPR does not fall to $\mathcal{O}(N^{-1})$, indicating that localization persists to some extent. However, the further we are from the roots, the closer the IPR gets to one predicted by thermalization.

Figure 5 shows plots of the long-time average (from

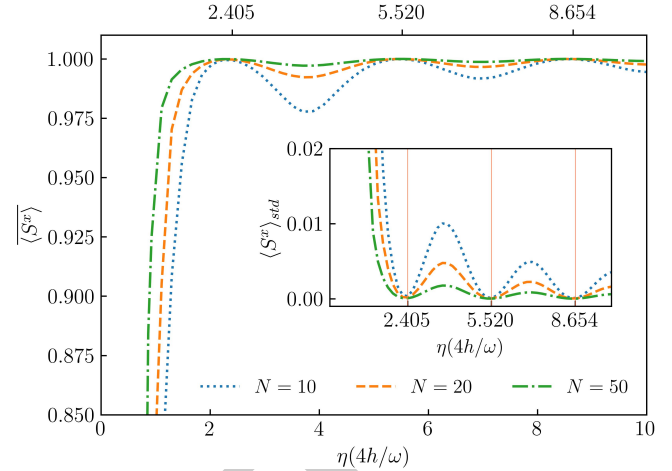


FIG. 5. Temporal average of $\langle \hat{S}^x \rangle$ (ordinate) for different η 's (abscissa) is plotted for $\sim 200T$ at higher ω for different $N=10, 20, 50$. $\langle \hat{S}^x \rangle$ is found to be unity at roots of $J_0(\eta)$. At points away from resonance points, $\langle \hat{S}^x \rangle$ falls below unity. The corresponding standard deviation $\langle \hat{S}^x \rangle_{std}$ supports the variation of $\langle \hat{S}^x \rangle$ (inset fig.). $\langle \hat{S}^x \rangle_{std}$ is ~ 0 describing a full freezing of the system at roots of $J_0(\eta)$ (red vertical solid lines).

$t = 0 - 200T$) of the field amplitude $\langle \hat{S}^x \rangle$ as a function of η . The system is started from the fully polarized state $s_n = N/2$ in the TSS and the dynamics simulated. The average is plotted for different values of amplitude h , keeping the frequency fixed at a high value of $\omega = 90$. It is clearly very close to unity at roots of $J_0(\eta)$ and falls at points away from it, indicating that S^x is approximately conserved at the localization points.

Small deviations do occur due to the role of higher order terms in the rotated Hamiltonian in eq 23. This can be demonstrated quantitatively by comparing the IPR obtained from the exact dynamics simulation with that obtained from the dynamics of $\tilde{H}(t)$ in eq. 23 after truncating the series at orders $k \geq 1$. This comparison can be seen in fig 6. The IPR plots from the exact dynamics indicate that the first localization point, represented by the lowest root of $J_0(\eta)$, does not show complete DMBL. However, DMBL is particularly conspicuous at large roots. The IPRs of the Floquet states obtained from the RWA dynamics exhibit large deviations from unity when away from the localization point as evidenced by the green and red curves in the middle panel of fig 6. However, complete localization is seen in the RWA dynamics at any localization point, in contrast to the exact case in the top panel. Thus, it is necessary to incorporate higher-order corrections into the Rotating Wave Approximation (RWA) at lower localization points. The application of the first-order

447 **III. PERSISTENCE OF DMBL IN THE CONTINUUM
448 LIMIT**

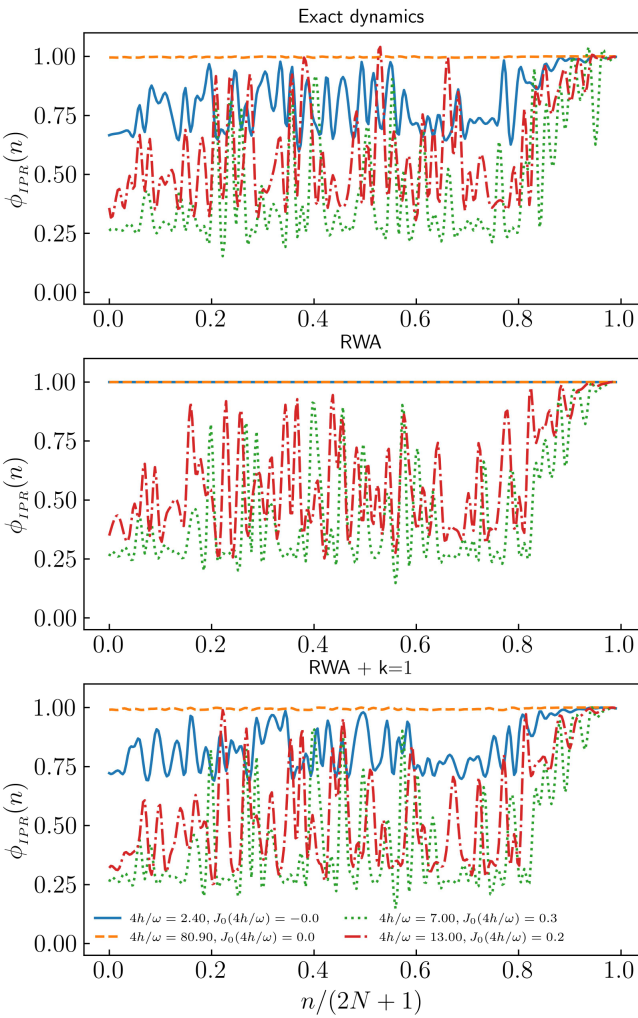


FIG. 6. The comparison between IPR for exact dynamics and RWA with corresponding correction orders. IPR is calculated for four different η 's and corresponding $J_0(\eta)$ values for colors, Blue : $\eta = 2.40, J_0(\eta) = 0.0$, dashed orange: $\eta = 80.9, J_0(\eta) = 0.0$, Green: $\eta = 7.0, J_0(\eta) = 0.3$, Red: $\eta = 13, J_0(\eta) = 0.2$. At low root of $J_0(\eta)$ IPR is not unity (Blue curve) while at higher root (orange dashed) it is unity while at points away from roots IPR are less than unity in the exact (top panel) plot. RWA does not matches with the exact plot. At all roots of $J_0(\eta)$ IPR is unity(middle panel). RWA with additional higher order terms exhibit similar system pattern(Bottom panel) with exact dynamics.

444 correction to RWA in the lower panel of fig 6 results in
445 a curve structure that is closer to that from the exact
446 dynamics.

449 In the continuum limit, where $N \rightarrow \infty$, the disparity
450 between neighboring values of s_i in equation 20 can
451 be disregarded, and s_i can be mapped to a continuum
452 $q \in [-1/2, 1/2]$ [55]. We define the Hamiltonian per
453 particle $h(t) \equiv \frac{H(t)}{N}$, and a canonically conjugate co-
454 ordinate $Np \equiv \left\langle -i \frac{\partial}{\partial q} \right\rangle$. Then, in this limit, the dynam-
455 ics can be approximated by that of a classical Hamil-
456 tonian [57]

$$h(t) = -2q^2 - [h \cos \omega t + h_0] \sqrt{1 - 4q^2} \cos p, \quad (28)$$

which yields the dynamical system

$$\begin{aligned} \frac{dq}{dt} &= \frac{\partial h}{\partial p} = h(t) \sqrt{1 - 4q^2} \sin p \\ \frac{dp}{dt} &= -\frac{\partial h}{\partial q} = 4q \left[1 - \frac{h(t) \cos p}{\sqrt{1 - 4q^2}} \right], \end{aligned} \quad (29)$$

457 where $h(t) = [h \cos \omega t + h_0]$. We have profiled simula-
458 tions of the ensuing dynamics with the *Poincaré sur-*
459 *face of section* (PSOS) of the full dynamics. Here, the
460 (q, p) -phase space is strobed at $t = nT$, and plotted
461 for a large number of initial conditions. The results
462 are shown in the upper panels of fig 7 for a small value
463 of $\omega = 2.0$ (left panel) and a large value $\omega = 90$ (right
464 panel). In both cases, the value of h is chosen such
465 that η lies on the first root of $J_0(\eta)$. The onset of chaos
466 for small drive frequency indicates thermal behaviour
467 for typical initial conditions, with small islands of reg-
468 ularity for others. This is consistent with similar re-
469 sults for small frequencies reported in [53, 58]. How-
470 ever, at high frequency, the regular islands distinctly
471 dominate over the chaos. The trajectories indicate
472 that the conservation of $\langle S^x \rangle \approx \sqrt{1 - 4q^2} \cos p$ [55]
473 at high ω persists in the thermodynamic limit. That
474 this is a signature of the underlying quantum dynam-
475 ics can be readily seen in the quantum phase space
476 representation of the Floquet Eigenstates for a large
477 but finite N . These are shown in the correspondingly
478 lower panels of fig 7. Here, we have plotted the Spec-
479 tral Average of the Husimi Q-functions of the acquired
480 Floquet States in the TSS. Specifically, for a coher-
481 ent state $|q, p\rangle$, the corresponding Spectral-Averaged
482 Husimi distribution [59] is obtained by

$$H(q, p) \equiv \frac{1}{(2N+1)\pi} \sum_n \langle q, p | \phi^n \rangle \langle \phi^n | q, p \rangle. \quad (30)$$

483 The quantum phase space retains signatures of the
484 classical phase space dynamics when $N = 100$, indi-
485 cating the onset of the persistence of S^x conserva-
486 tion that arises from the resonance condition at high fre-
488 quencies.

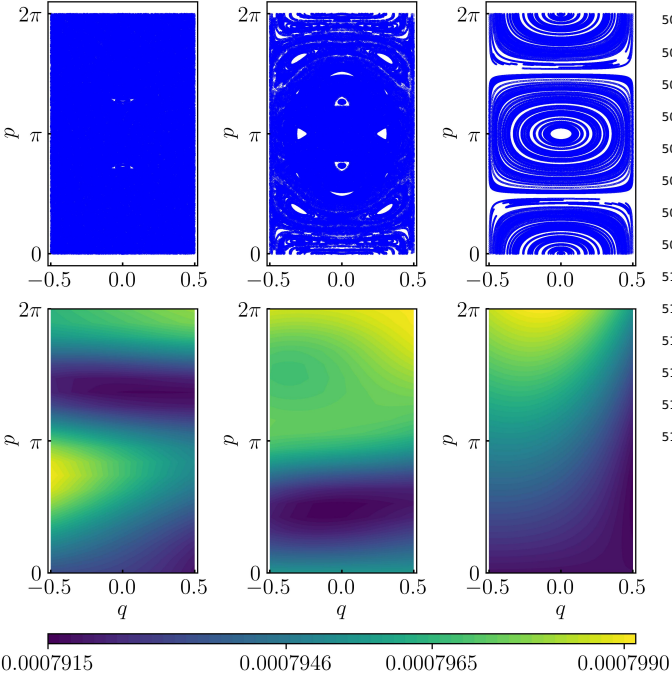


FIG. 7. Phase-space distributions at $\omega = 1.0$ (left panels), $\omega = 2.5$ (middle panels) and $\omega = 90.0$ (right panels) for 100 initial conditions. The drive amplitude h is always adjusted such that $\eta = 4h/\omega$ lies on the smallest root of $J_0(\eta)$, i.e. $\eta = 2.4048\dots$. At small $\omega = 1.0$, the classical PSOS, obtained from simulating the dynamics in eqns 29 (top left panel), shows chaotic behaviour, and at $\omega = 2.5$, regular regions start to appear. At higher $\omega = 90.0$, the dominance of regular dynamics can be readily seen (top right panel). The bottom panels plot the corresponding Spectral-Averaged Husimi-Q function, obtained from the Floquet modes $|\phi^n\rangle$ using eqn. 30, and setting $N = 100$. The $\omega = 1.0$ case (bottom left panel) has a dispersed distribution in colour. This is consistent with the chaotic behaviour seen in the continuum limit. At $\omega = 2.5$ (bottom middle panel), there is a partial regular pattern observed together with a dispersed pattern. In the $\omega = 90$ -case (bottom right panel), the distribution has distinct colour contrasts, which is consistent with the regular dynamics pattern seen in the continuum limit.

489 IV. PHASE CROSSOVER FROM THERMAL TO DMBL

490 The analysis of the periodically driven LMG model
491 reveals two distinct scenarios at low and high external
492 drive frequencies. In the former case, thermalization
493 in accordance with FETH is seen, whereas in the latter
494 case, DMBL is induced. As a result, we hypothesize
495 that a macroscopic change in phase occurs due to the
496 influence of frequency.

497 To demonstrate this, we investigate the IPR of the
498 Floquet mode with smallest quasienergy for numerous
499 frequencies and system sizes, along with the associ-
500 ated drive amplitude h keeping the system at a local-
501 ization point. The results are shown in fig 8 . In the

502 low-frequency range $\omega \in [1.0, 9.0]$, the IPR exhibits val-
503 ues well below unity. Moreover, the IPR gradually di-
504 minishes with increasing system size, following a sys-
505 tem size inverse proportional trend, which confirms
506 the participation distribution (as shown in the bottom
507 panel). As the limit $N \rightarrow \infty$, the inverse participation
508 ratio (IPR) tends towards zero, indicating a fully de-
509 localized state. The plots reveal a gradual increase
510 in the unity of IPR over a certain frequency range,
511 specifically at $\omega \approx 5$. In addition, the rise does not
512 cross with those for different values of N , suggesting
513 the onset of a phase crossover [41, 60]. As the size of
514 the system increases, the crossover region becomes
515 smoother, rather than sharper.

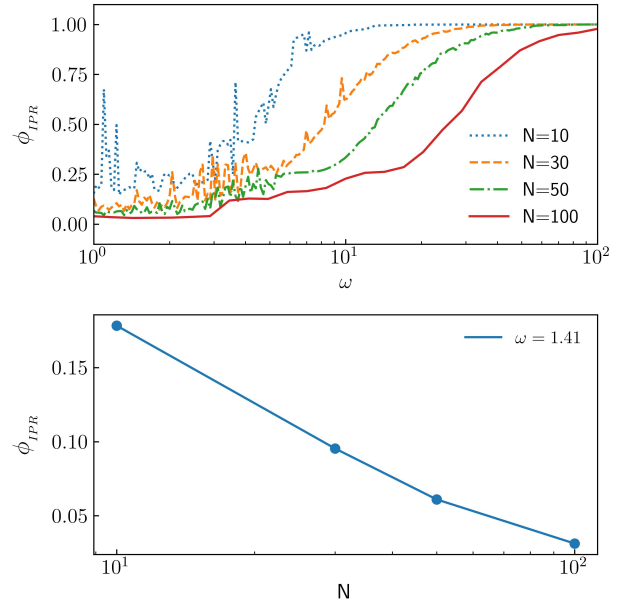


FIG. 8. IPR is plotted (top panel, ordinate) for a range of $\omega \in [1, 100]$ (top panel, abscissa) for four different $N = 10, 30, 50, 100$ at root of $J_0(\eta)$. At small ω upto $\omega \sim 10$ IPR founds to be very small and rises slowly upto unity (fully localized) at higher frequencies. At bottom panel IPR (ordinate) is plotted for different $N = 10, 30, 50, 100$ (bottom panel, abscissa) for a random small $\omega \sim 1$ at root of $J_0(\eta)$ from the values from top panel. IPR falls as inversely proportional to N , indicating an approach to a fully distributed (thermal) state. The smooth rise in IPR defines a phase crossover (top panel) between a fully thermal phase to a fully localized phase.

517
518 We can also look at this crossover more clearly in
519 the plots of the heating rate of the system, defined
520 simply by the expectation value of the Hamiltonian,
521 $\langle \hat{H}(t) \rangle$. We have carried out the numerical evalua-
522 tion from the simulated dynamics over $t = 500T$.
523 When the system is adequately described by FETH,
524 the temporal fluctuations in the heating rate, defined

525 by $\langle H \rangle_{std}^2 \equiv \overline{\langle \hat{H} \rangle^2} - \overline{\langle \hat{H} \rangle}^2$ (see eqn 3), are minimal in
 526 the thermodynamic limit, as the spread of states leads
 527 to a limited standard deviation[61]. Conversely, the
 528 onset of athermalism is indicated by nonzero fluctua-
 529 tions in time. If we set the initial state to the fully po-
 530 larized state in the TSS (given by $|s_N\rangle$), then the onset
 531 of freezing, together with DMBL, will result in nearly
 532 infinite hysteresis in the ensuing dynamics, causing
 533 $|\psi\rangle(t) \approx |s_N\rangle \forall t$. From eqn. 17, we can clearly see
 534 that this will lead to a linearly rising dependence on
 535 ω in $\langle H \rangle_{std}$ as long as we stick to a localization point
 536 given by a fixed h/ω . All these observations are cor-
 537 roborated by the heating rate plots in figure 9.

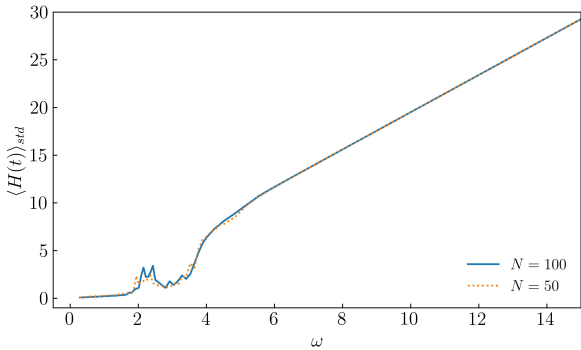


FIG. 9. The standard deviation of the heating rate, denoted by $\langle H \rangle_{std}$, calculated over a span of $t = 500T$ for two system sizes. Here, h is varied to keep $\eta = 4h/\omega$ at the first root of $J_0(\eta)$. A nonsingular rise has been identified at $\omega \approx 4.0$. $\langle H \rangle_{std}$ exhibits a diminutive magnitude below that value of ω , while a linear rise is observed at higher frequencies, consistent with freezing. A vanishingly small standard deviation for $\omega \ll 4.0$ indicates the presence of a thermal region, whereas a larger finite standard deviation suggests the existence of athermal behaviour. The small peaks observed at $\omega \in [2, 4]$ are finite-size effects that disappear in the thermodynamic limit.

538

539

V. CONCLUSION AND OUTLOOK

541 We have delved into the onset of freezing and
 542 phase cross-over in 1D spin systems driven by a time-
 543 periodic transverse field, contrasting the responses
 544 in the Transverse Field Ising Model (TFIM) with that
 545 of the long-range Lipkin-Meshkov-Glick Model (LMG).
 546 The parametrization of DMBL is based on the Inverse
 547 Participation Ratio (IPR) of the Floquet eigenstates.
 548 Our investigations compared the IPRs from both mod-
 549 els numerically, and found the emergence of thermal
 550 behavior at low frequencies and freezing at high fre-

551 quencies for the LMG model, the latter a direct conse-
 552 quence of the appearance of additional approximately
 553 conserved quantities.

554 Long-range spins exhibit strong localization in spin-
 555 coordinate space for the LMG model when the drive
 556 frequency is $\omega \gg J$, where J represents the spin ex-
 557 change energy. The localization of the LMG model
 558 occurs at specific resonance points of the drive fre-
 559 quency ω and amplitude h , at $J_0(4h/\omega) = 0$, $\omega \gg J$.
 560 This is apparently similar to the phenomenon of Dy-
 561 namical Freezing (DMF) in the Transverse Field Ising
 562 Model (TFIM), where comparable localization at res-
 563 onance points, determined by the roots of $J_0(2h/\omega)$,
 564 occurs due to the onset of an additional approximate
 565 conservation in the transverse field itself. However,
 566 a key difference is the thermal behaviour of the LMG
 567 model at low frequencies. Plots of the IPR for a range
 568 of frequencies along the resonance manifold exhibits
 569 a smooth increase in IPR yielding a quantum phase-
 570 crossover from a thermal phase governed by the Flo-
 571 quet Eigenstate Thermalization Hypothesis (FETH) to
 572 a Dynamically Many-Body localized phase (DMBL).
 573 This crossover is absent in the TFIM, as can be readily
 574 seen in the significant magnitude of the inverse par-
 575 ticipation ratio (IPR) even at low frequencies. Thus,
 576 the suppression of thermalization through Dynamical
 577 Many Body Localization in long-range systems can be
 578 controlled via Floquet engineering, even in clean sys-
 579 tems without any disorder. Thus, periodically driven
 580 long-range spin systems are an excellent tool for in-
 581 vestigating disorder-free Many Body Localization, as
 582 can be readily seen via the IPR of its Floquet modes.
 583 There are several unexplored indicators of DMBL,
 584 such as entanglement entropy and level statistics [10],
 585 which we defer to future studies. In addition,
 586 Halpern in 2019 proposed a quantum engine based
 587 on MBL[11] which works between strong localized
 588 and thermal phases of the system. In our proposed
 589 LMG model, tuning the system parameters by bring-
 590 ing them to the resonance points, then adiabatically
 591 cycling the frequency from the thermal region to the
 592 DMBL region, can achieve a similar engine without
 593 going through a phase transition.

A. Acknowledgements:

595 One of the authors, MR acknowledges The Univer-
 596 sity of Burdwan for support via a state-funded fel-
 597 lowship. AR acknowledges support from the Uni-
 598 versity Grants Commission (UGC) of India, via BSR
 599 Startup Grant No. F.30-425/2018(BSR), as well as
 600 from the Science and Engineering Research Board
 601 (SERB) Core Research Grant No. CRG/2018/004002.

- [1] S. Bordia Pranjal, Lüschen Henrik, *Nature Physics* **13**, 460 (2017).
- [2] S. Sahoo, I. Schneider, and S. Eggert, Periodically driven many-body systems: A floquet density matrix renormalization group study (2019), arXiv:1906.00004 [cond-mat.str-el].
- [3] A. Das, *Phys. Rev. B* **82**, 172402 (2010).
- [4] G. B. Mbeng, A. Russomanno, and G. E. Santoro, The quantum ising chain for beginners (2020), arXiv:2009.09208 [quant-ph].
- [5] H. S. Yamada and K. S. Ikeda, *Phys. Rev. E* **105**, 054201 (2022).
- [6] A. Roy and A. Das, *Phys. Rev. B* **91**, 121106 (2015).
- [7] H. Li, B. Shapiro, and T. Kottos, *Phys. Rev. B* **98**, 121101 (2018).
- [8] A. Eckardt and E. Anisimovas, *New Journal of Physics* **17**, 093039 (2015).
- [9] L. Zhang, V. Khemani, and D. A. Huse, *Phys. Rev. B* **94**, 224202 (2016).
- [10] V. Khemani, A. Lazarides, R. Moessner, and S. L. Sondhi, *Phys. Rev. Lett.* **116**, 250401 (2016).
- [11] N. Yunger Halpern, C. D. White, S. Gopalakrishnan, and G. Refael, *Phys. Rev. B* **99**, 024203 (2019).
- [12] T. Nag, S. Roy, A. Dutta, and D. Sen, *Phys. Rev. B* **89**, 165425 (2014).
- [13] G. Carleo, F. Becca, M. Schiró, and M. Fabrizio, *Scientific Reports* **2**, 243 (2012).
- [14] S. Aditya and D. Sen, Dynamical localization and slow thermalization in a class of disorder-free periodically driven one-dimensional interacting systems (2023), arXiv:2305.06056 [cond-mat.stat-mech].
- [15] M. Schiulaz, A. Silva, and M. Müller, *Phys. Rev. B* **91**, 184202 (2015).
- [16] T. Grover and M. P. A. Fisher, **2014**, P10010.
- [17] Z. Papić, E. M. Stoudenmire, and D. A. Abanin, *Annals of Physics* **362**, 714 (2015).
- [18] A. Smith, J. Knolle, D. L. Kovrizhin, and R. Moessner, *Phys. Rev. Lett.* **118**, 266601 (2017).
- [19] O. Hart, S. Gopalakrishnan, and C. Castelnovo, *Phys. Rev. Lett.* **126**, 227202 (2021).
- [20] H. Lipkin, N. Meshkov, and A. Glick, *Nuclear Physics* **62**, 188 (1965).
- [21] N. Meshkov, A. Glick, and H. Lipkin, *Nuclear Physics* **62**, 199 (1965).
- [22] A. Glick, H. Lipkin, and N. Meshkov, *Nuclear Physics* **62**, 211 (1965).
- [23] P. Ribeiro, J. Vidal, and R. Mosseri, *Phys. Rev. E* **78**, 021106 (2008).
- [24] N. Debergh and F. Stancu, *Journal of Physics A: Mathematical and General* **34**, 3265 (2001).
- [25] P. Titum and M. F. Maghrebi, *Phys. Rev. Lett.* **125**, 040602 (2020).
- [26] A. Campa, T. Dauxois, and S. Ruffo, *Physics Reports* **480**, 57 (2009).
- [27] E. R. S. Eisele, Theodor, *Journal of Statistical Physics*, 161 (1988).
- [28] A. Canning, *Physica A: Statistical Mechanics and its Applications* **185**, 254 (1992).
- [29] D. Vu, K. Huang, X. Li, and S. Das Sarma, *Phys. Rev. Lett.* **128**, 146601 (2022).
- [30] G. Misguich, V. Pasquier, and J.-M. Luck, *Phys. Rev. B* **94**, 155110 (2016).
- [31] M. Calixto and E. Romera, *Journal of Statistical Mechanics: Theory and Experiment* **2015**, P06029 (2015).
- [32] K. Fujii, *Journal of Modern Physics* **8**, 2042 (2017).
- [33] D. A. Abanin, E. Altman, I. Bloch, and M. Serbyn, *Rev. Mod. Phys.* **91**, 021001 (2019).
- [34] M. Srednicki, *Phys. Rev. E* **50**, 888 (1994).
- [35] M. Srednicki, *Journal of Physics A: Mathematical and General* **32**, 1163 (1999).
- [36] M. Holthaus, *Journal of Physics B: Atomic, Molecular and Optical Physics* **49**, 013001 (2015).
- [37] M. Vogl, M. Rodriguez-Vega, and G. A. Fiete, *Phys. Rev. B* **101**, 024303 (2020).
- [38] M. Bukov, L. D'Alessio, and A. Polkovnikov, *Advances in Physics* **64**, 139 (2015).
- [39] L. D'Alessio and M. Rigol, *Phys. Rev. X* **4**, 041048 (2014).
- [40] R. Yousefjani, S. Bose, and A. Bayat, *Phys. Rev. Res.* **5**, 013094 (2023).
- [41] P. Sierant, M. Lewenstein, A. Scardicchio, and J. Zakrzewski, *Phys. Rev. B* **107**, 115132 (2023).
- [42] R. Yousefjani, S. Bose, and A. Bayat, *Phys. Rev. Res.* **5**, 013094 (2023).
- [43] F. Alet and N. Laflorencie, *Comptes Rendus Physique* **19**, 498 (2018).
- [44] S. J. Garratt and S. Roy, *Phys. Rev. B* **106**, 054309 (2022).
- [45] R. B. Stinchcombe, *Journal of Physics C: Solid State Physics* **6**, 2459 (1973).
- [46] F. E. H. George Arfken, Hans Weber, *Mathematical Methods for Physicists*, 7th ed. (Academic Press).
- [47] S. Mukherjee, A. Spracklen, D. Choudhury, N. Goldman, P. Öhberg, E. Andersson, and R. R. Thomson, *New Journal of Physics* **17**, 115002 (2015).
- [48] S.-H. Lin, B. Sbierski, F. Dorfner, C. Karrasch, and F. Heidrich-Meisner, *SciPost Phys.* **4**, 002 (2018).
- [49] N. C. Murphy, R. Wortis, and W. A. Atkinson, *Phys. Rev. B* **83**, 184206 (2011).
- [50] E. J. Torres-Herrera, I. Vallejo-Fabila, A. J. Martínez-Mendoza, and L. F. Santos, *Phys. Rev. E* **102**, 062126 (2020).
- [51] N. Trivedi and D. Heidarian, *Progress of Theoretical Physics Supplement* **160**, 296 (2005).
- [52] G. Misguich, V. Pasquier, and J.-M. Luck, *Phys. Rev. B* **94**, 155110 (2016).
- [53] A. Russomanno, R. Fazio, and G. E. Santoro, *Europhysics Letters* **110**, 37005 (2015).
- [54] N. Defenu, T. Enss, M. Kastner, and G. Morigi, *Phys. Rev. Lett.* **121**, 240403 (2018).
- [55] T. Mori, *Journal of Physics A: Mathematical and Theoretical* **52**, 054001 (2019).
- [56] J. Johansson, P. Nation, and F. Nori, *Computer Physics Communications* **184**, 1234.
- [57] B. Sciolla and G. Biroli, *Phys. Rev. Lett.* **105**, 220401 (2010).

- ⁷¹⁸ [58] R. A. Kidd, M. K. Olsen, and J. F. Corney, Phys. Rev. A ⁷³⁴ [66] A. Haldar and A. Das, Annalen der Physik **529**,
⁷¹⁹ **100**, 013625 (2019). ⁷³⁵ 1600333.
- ⁷²⁰ [59] A. Bäcker, S. Fürstberger, and R. Schubert, Phys. Rev. ⁷³⁶ [67] J. M. Deutsch, Phys. Rev. A **43**, 2046 ().
⁷²¹ E **70**, 036204 (2004). ⁷³⁷ [68] E. W. Hobson, On the Second Mean-Value Theorem of
⁷²² [60] S. Sachdev, *Quantum Phase Transitions*, 2nd ed. (Cam- ⁷³⁸ the Integral Calculus (1909).
⁷²³ bridge University Press, Cambridge, 2011). ⁷³⁹ [69] M. Rigol and M. Srednicki, Physical Review Letters
⁷²⁴ [61] P. Reimann, Journal of Statistical Mechanics: Theory ⁷⁴⁰ **108**, 10.1103/physrevlett.108.110601 (2012).
⁷²⁵ and Experiment **2021**, 103106 (2021). ⁷⁴¹ [70] J. M. Deutsch, IOP Publishing Ltd **81**, 296 ().
⁷²⁶ [62] L. Reichl, *The Transition to Chaos: Conservative Clas- ⁷⁴² [71] R. Nandkishore and D. A. Huse, Annual Re-
⁷²⁷ sical and Quantum Systems, Fundamental Theories of ⁷⁴³ view of Condensed Matter Physics **6**, 15 (2015),
⁷²⁸ Physics, Vol. 200 (Springer International Publishing). ⁷⁴⁴ <https://doi.org/10.1146/annurev-conmatphys-031214-014726>.*
- ⁷²⁹ [63] N. Srivatsa, R. Moessner, and A. E. Nielsen, Phys. Rev. ⁷⁴⁵ ⁷⁴⁶ [72] L. D'Alessio and A. Polkovnikov, **333**, 19.
⁷³⁰ Lett. **125**, 240401. ⁷⁴⁷ [73] S. Notarnicola, F. Iemini, D. Rossini, R. Fazio, A. Silva,
⁷³¹ [64] Quantum ising phase transition. ⁷⁴⁸ and A. Russomanno, Phys. Rev. E **97**, 022202 (2018).
⁷³² [65] B. Marcos, A. Gabrielli, and M. Joyce, Open Physics **10**, ⁷⁴⁹ [74] A. Lazarides, A. Das, and R. Moessner, Phys. Rev. Lett. ⁷⁵⁰ **115**, 030402 (2015).

DRAFT